Dose and dose rate measurements in proton beams using the luminescence of beryllium oxide

Teichmann, T.; Torres, M. J. Gonzalez; van Goethem, M. J.; van der Graaf, E. R.; Henniger, J.; Jahn, A.; Kiewiet, H. H.; Sommer, M.; Ullrich, W.; Weinhold, C.

Published in:
Journal of Instrumentation

DOI:
10.1088/1748-0221/13/10/P10015

Publication date:
2018

Prepared for submission to JINST

Dose and dose rate measurements in proton beams using the luminescence of beryllium oxide

T. Teichmann,[a,b] **M.J. Gonzalez Torres,**[a] **M.J. van Goethem,**[c] **E.R. van der Graaf,**[c] **J. Henniger,**[a] **A. Jahn,**[b] **H.H. Kiewiet,**[c] **M. Sommer,**[b] **W. Ullrich,**[b] **C. Weinhold**[a] **and T. Kormoll**[a]

[a] *Technische Universität Dresden, Zellescher Weg 19, 01062 Dresden, Germany*
[b] *GWT-TUD GmbH, Freiberger Str. 33, 01067 Dresden, Germany*
[c] *KVI – Center for Advanced Radiation Research, Zernikelaan 25, 9747AA Groningen, The Netherlands*

E-mail: tobias.teichmann@tu-dresden.de

Abstract: The present work investigates methods for dose and dose rate measurements in proton beams using the luminescence of beryllium oxide (BeO). Experiments are carried out to determine the response of the optically stimulated luminescence (OSL) of BeO as well as the radioluminescence (RL) of BeO within the depth dose profile of a 190 MeV scattered proton beam. The acquired data is compared to an ionization chamber reference and a Monte Carlo simulation. Both dose readings from the RL and OSL measurements show accurate values in the entrance path with an increasing underestimation in the high LET region of the Bragg peak. The amount of this quenching is different for RL and OSL so that the ratio of RL to OSL dose measurements opens venues to correct the measurements to the accurate dose.

Keywords: Dosimetry concepts and apparatus, Solid state detectors, Instrumentation for particle-beam therapy, Scintillators and scintillating fibres and light guides

[1]Corresponding author.

Contents

1 Introduction

The application of proton beams for external radiotherapy experiences a strong increase. Its advantages compared to conventional photon therapy – better spatial precision and higher dose deposition in the treatment volume – lead to successful applications, e.g. in pediatric treatments and treatments of prostate cancer. This goes in hand with an increased demand for dosimetric systems with high spatial resolution and a linear dose response, especially for the high LET in the Bragg peak region, for quality control and online monitoring of organs at risk.

In order to keep the overall dosimetric treatment uncertainty below the 5% margin recommended by the IAEA [1], a maximum uncertainty of 1% on the actual dose measurement is advised. This requirement can be met by an ionization chamber attached with high fidelity cables to an accurate electrometer. Due to its mostly LET independent response, the ionization chamber is the reference system for hadron therapy dose and dose rate measurements. However, the relatively large sensitive volume compromises its applicability in very small and narrow fields. Additionally, changes in air temperature and pressure must be accounted for.

Solid state detectors can overcome these limitations and provide spatially highly resolved dose and dose rate measurements with the required accuracy. Among possibly suitable detectors, there are radiochromic films [2], alanine detectors [3] and polymer gel dosimeters [4]. The challenge of these devices is their LET dependent response which leads in most cases to an underestimation of the dose in the Bragg peak region. There are indications that diode detectors, when specially pre-irradiated, can yield an LET independent signal and can be used for relative measurements, e.g. to record the shape of a depth dose curve [5].

A solid state detector with which an LET independent response can be reached is the diamond detector. Commercially available detectors have successfully been applied to absolute dosimetry with the required accuracy [6].

Complementary to diamond detectors, this work investigates the use of probes based on the radioluminescence (RL) and optically stimulated luminescence (OSL) of beryllium oxide (BeO).

BeO is a well-known luminescent material with excellent tissue equivalence for photon and electron radiation [7–10]. The material is used as an OSL detector in personal and scientific dosimetry systems for more than a decade [11–18]. The RL of BeO has been shown to be linear to the applied dose rate in photon fields [19]. The combination of RL and OSL measurements has been tested in photon fields [20, 21], with probes attached to optical fibers. Dose and dose rate measurements were possible after a proper treatment of the light which is generated in the fiber itself. The pulsed character of accelerator induced beams allows a temporal discrimination of this so called "stem effect" which appears promptly from the RL and OSL light which has a time constant of approximately 30 µs [21].

It is known from photon irradiation that the OSL response of BeO is dependent on the energy of the secondary electrons and thereby the LET. The sensitivity is decreasing with higher LET – referred to as quenching in the following. The aim of this work is to quantify the amount of quenching in the RL signal of BeO as well as in the OSL of BeO in proton fields and to investigate possible means of detecting and correcting the quenching.

In the simplest model, the effect of quenching is caused by local saturation of the available luminescence centers, so that not all locally deposited energy leads to populated traps and thereby to luminescence light. The decrease of the signal M with increasing stopping power S can be described by the semi-empirical Birks' model [22, 23]:

$$M = \frac{M_0}{1 + k_\mathrm{B} S}$$

M_0 is the unquenched signal which is not affected by the density of available states. k_B is a material and process specific parameter. Birks' law is formulated and well tested for organic scintillators. Although it has been applied to inorganic scintillators [24], its applicability to (stimulated) luminescence of BeO is not necessarily accurate. It will however serve as a test for plausibility and thereby verify that an observed decrease in the signal can be attributed to quenching. Since the mechanisms of RL and OSL in BeO happen at different luminescence centers with different densities of states, RL and OSL have to be treated individually.

Quantification and correction of the quenching effect will have a major impact on the feasibility of OSL and RL for dose and dose rate measurements in proton fields.

2 Materials and methods

Irradiation has been performed at the AGOR cyclotron, KVI-CART, University of Groningen, The Netherlands. The superconducting AGOR cyclotron accelerates protons up to 190 MeV with a

frequency range of 24-62 MHz [25]. Details about the setup of the proton beam line can be found in [26].

The primary beam leaving the vacuum passes through a double scatter setup (1.44 mm Pb; 0.9 mm W) in order to provide a flat irradiation field at the location of the phantom [26]. Before the scatter setup, ionization chambers are used as beam intensity monitors (BIM) to measure the fluence [26]. This is followed by a field shaping collimator. This beamline setup causes a non monoenergetic proton beam with a second small peak in a lower depth than the position of the main Bragg peak. The interactions undergone by the protons in the beamline produce also other secondary particles which contribute to the dose deposition. The diameter of the proton beam at the target position is 7 cm.

The irradiated phantom is made out of 20 PMMA slabs (100 mm × 100 mm × 10 mm, density 1.18 g/cm^3) stacked horizontally in a 30 cm L-bracket (also PMMA). An additional block of PMMA (100 mm × 100 mm × 50 mm) is fixed on the bracket to ensure the correct placement of the slabs. Different adapter slabs can be exchanged with the slabs of the phantom to place a Markus chamber (PTW Freiburg), the OSL detectors or the RL probes in the center of the beam profile at different depths inside the PMMA phantom. The assembly with the different adapters is displayed in figure 1.

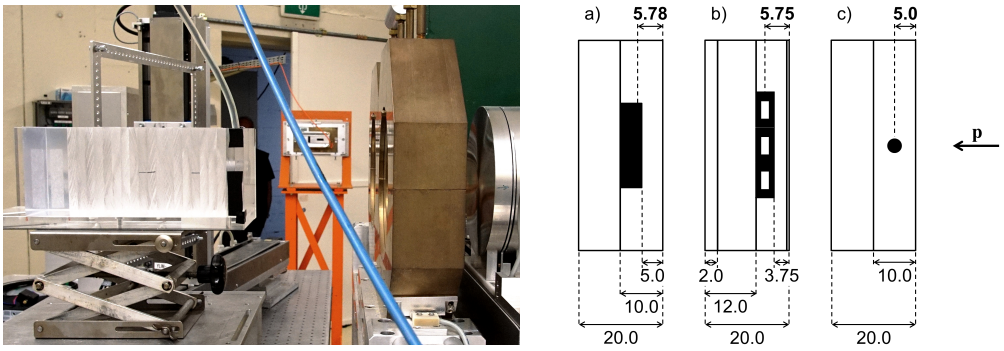

Figure 1. Irradiation setup for the PMMA phantom with Markus chamber (left) and drawings of the adapters for Markus chamber a), OSL b) and RL probes c). View from top, incident protons from the right side, all dimensions are in mm. The reference depth of the sensitive volume is indicated in bold in the top right corner for each drawing.

The BIM has been calibrated with the Markus chamber. In each irradiation, 10.2 mGy were delivered at the first position of the Markus chamber, i.e. at a depth of 5.78 mm. At the given amplification this corresponds to 10^6 monitor units (MMU). Assuming that the BIM acts as a counting device, the relative uncertainty (one standard deviation) of the delivered dose is therefore 1/1000.

2.1 OSL setup

The setup for the OSL measurements with BeO is displayed in figure 2. The 4.7 mm × 4.7 mm × 0.5 mm BeO detectors (Thermalox 995, Materion, density 3.02 g/cm^3) used in this experiment have been described in previous publications [10, 17].

Nine detectors have been placed in a 3 × 3 frame. The center of the sensitive volume of the detectors was 5.75 mm from the surface which corresponds to the sensitive depth of the Markus

chamber at 5.78 mm. Each measurement in a certain depth has been done with fresh detectors in order not to accumulate dose and compromise the measurements by saturation effects. Prior to the experiments, each detector has been individually calibrated with a ^{137}Cs source at a calibration dose of 10 mGy.

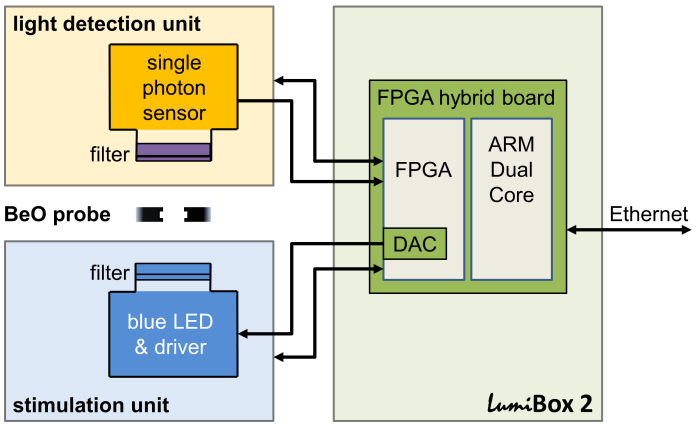

Figure 2. Setup of the OSL system.

The detector read out system is a new development. A modulated stimulation of the BeO detectors is performed by a blue LED (Oslon SSL 80, Osram) with a center wavelength of 450 nm. A single photon sensor (H10682-210, Hamamatsu) detects the OSL signal on the opposite side of the BeO detector. Additional optical filtering is used to separate stimulation and luminescence light. A blue band pass (ET 445/30, Chroma Technology Corp.) and an edge filter (GG420, Schott AG) are placed in front of the BeO and UV band pass filters (UG11 and DUG11, Schott AG) are located in front of the single photon sensor.

The single photon events from the photon sensor are sampled by an FPGA hybrid board as described in [27]. The analysis of the generated time stamp raw data is based on a rectangular weighting approach considering the time dependent structure of the signal due to the modulated stimulation. The method includes zero dose subtraction and dead time correction as well as a correction of other photon sensor related parasitic effects.

In addition to the dose, the uncertainty is calculated based on assumption that each measurement of single photons is a Poisson process and obeys the corresponding statistical laws. In the total dose uncertainty, the counting uncertainty of the actual measurement, the foregoing measurement of the zero signal and the calibration are included. The intensity and time duration of the stimulation have been chosen in order to achieve 2% (2σ) or less at a 10 mGy measurement which is in the range of a required accuracy of a potentially clinically applicable system.

2.2 RL setup

The RL measurements have been performed using a cylindrical BeO ceramic (height 1 mm, diameter 1 mm, Thermalox 995, Materion). The luminescent detector is coupled to a PMMA light guide (diameter 1 mm, length 15 m, LEONI Fiber Optics) by transparent epoxy resin (EPO-TEK 301-2, Epoxy Technology). The assembly is encapsulated in light tight epoxy resin (EPO-TEK 320, Epoxy Technology). Heat shrinking tube is added to increase the mechanical resilience. The light guide

is surrounded by black PE cladding with 2.2 mm diameter. A second probe without a luminescent detector is used as a reference to eliminate the stem effect, i.e. the luminescent signal which is generated due to the irradiation of the light guide. The probes are coupled directly to a single photon sensor (H10682-210, Hamamatsu) by an SMA 905 fiber connector. No additional optical filtering of the luminescence light is applied. The signal of the photon sensor was transmitted out of the irradiation room by a BNC connection. The counting of the single photon events was performed by an FPGA connected to a PC with dedicated LabVIEW Software which was located in the control room. The setup for the RL measurements is displayed in figure 3.

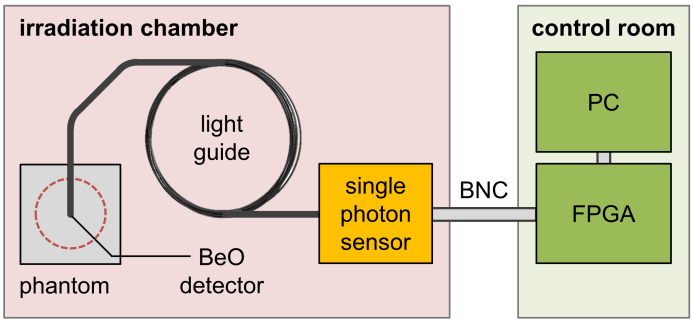

Figure 3. RL measurement setup. View on the phantom in the direction of irradiation. The red circle indicates the lateral borders of the primary proton beam.

The calibration of the system has been done in advance with a ^{137}Cs source (28 mGy h^{-1}) at TU Dresden. A measurement without any connected probe has been performed to evaluate the signal of the single photon sensor which remained at a fixed position with low dose rate inside the irradiation room during all irradiations. The dark count signal of the single photon sensor without any irradiation was negligible ($< 2\,s^{-1}$) for all RL measurements.

2.3 Simulations

The simulations were performed with the Monte Carlo transport program FLUKA [28, 29] using HADROTHErapy as default settings. The delta ray production and the particle transport threshold were set to 100 keV, except for neutron transport which was set down to thermal energies. A flat and circular beam (at 15 cm from the phantom entrance) was chosen similar to the one at the AGOR irradiation facility [26].

In order to reproduce the experimental irradiations, the proton beam was defined using the energy fluence spectrum of protons before the phantom entrance. Secondary photons and neutrons produced by proton interactions in the beamline are of particular interest for the present work and their respective energy fluence spectra were also included in the beam definitions. The resulting energy spectrum was adjusted to reproduce the Markus chamber measurements in PMMA.

The setup for the PMMA and OSL irradiations (figure 1) were reproduced in the simulations. The ionization potential values used for protons in PMMA and BeO were 74.0 and 93.2 eV, respectively. The scoring mesh for the dose deposition was set equal to the detector size in each setup. The number of primaries were 5×10^6 for the proton spectra and 5×10^7 for neutron and photon spectra for all simulations.

3 Results

3.1 OSL measurements

At each depth, nine OSL dosimeters have been irradiated at once. In table 1 of the appendix, all dose readings from the OSL dosimeters are shown. The OSL measurements at one depth are uniform within the uncertainty of each measurement of approximately 2% (2σ). In the entrance path this confirms the spatial uniformity which is achieved with the double scattering setup. At larger depth where there is an underestimation of the OSL dose – which is examined in the next section in detail – the uniformity persists which indicates that the quenching is due to fundamental properties like the density of available states like formulated in Birks' law. In contrast, the sensitivity, i.e. the amount of luminescence light due to a given dose, varies largely among the dosimeter ensemble. The dosimeters are individually sintered ceramics chips which may have very different optical properties in terms of scattering and absorption. After calibration, these optical differences are accounted for so that the observed quenching in terms of a reduction of measured dose can be attributed to processes in the band structure alone. In the following analysis, only the mean dose value at a certain depth is considered.

3.2 Simulation and comparison

Figure 4 compares the results of the OSL and RL measurements with the Markus chamber reference. Assuming Bragg-Gray conditions, the OSL and RL results have been scaled with the mass stopping powers to the dose in PMMA. In this approximation the mass stopping powers were obtained using the PSTAR database from NIST [30] for PMMA and the stopping power calculator from SR-NIEL [31] for BeO with iteratively calculated values for the remaining proton energy at each depth in the phantom assuming mono-energetic primary protons.

The scaled OSL and RL curves are in very good agreement with the reference regarding the entrance dose in the low LET region up to 7 cm. The position of the main Bragg peak at 19 cm can also be reproduced by all three measurement methods. Due to the scatter setup of the beam there is a lower energy component in the primary beam which causes the second Bragg peak at approximately 12.5 cm. This feature is also present in both the OSL and RL measurements and the reference. Going to larger depths the OSL and RL measurements suffer from an underestimation of the dose, i.e. quenching, which is caused by a raise in LET.

The Markus chamber measurement serves as a reference for the simulation, which has been adapted to reproduce the measured shape. In figure 5, the simulated and the measured depth dose curve in PMMA are shown. They have been brought into agreement in the peak region and the secondary peak. There is only a very slight underestimation of the simulation in the entrance path. Secondary particles in the scatterers and the collimators have been considered, but no from supporting structure which is not directly hit by the beam. Radiation emerging from such components or inaccuracies in the physical models might cause this minimal underestimation.

In a second set of simulations the dose in BeO has been scored. Figure 6 displays the resulting total dose in BeO in comparison with the measurements. The entrance dose and the positions of the Bragg peaks are in well agreement. For values at larger depths, there is a considerable underestimation of the measured signals, which is studied in more detail in the next section.

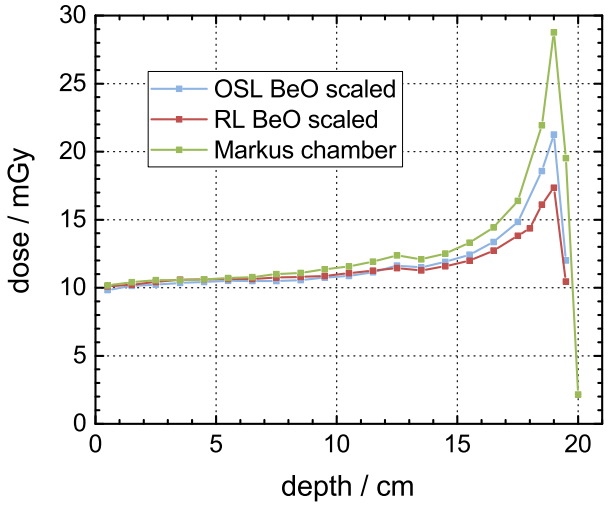

Figure 4. Dose depth curve measurements with OSL and RL of BeO, scaled with the mass stopping powers to the dose in PMMA (Bragg-Gray approximation). Markus chamber measurement as reference.

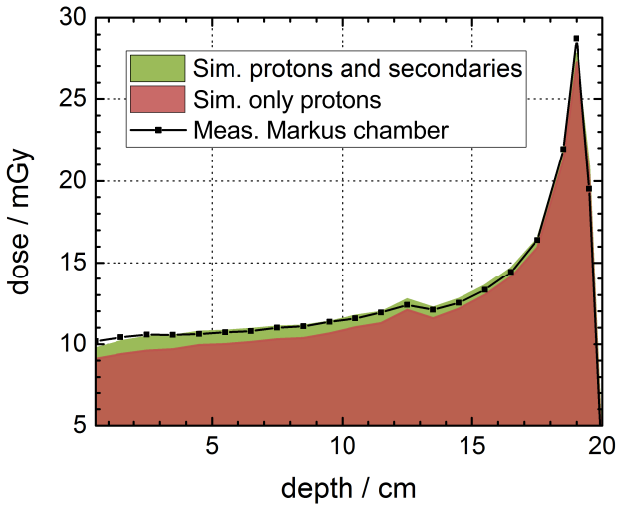

Figure 5. Dose depth curve comparison: Markus chamber measurement and simulation of dose in PMMA. Optimization of the modelled radiation field in the simulation.

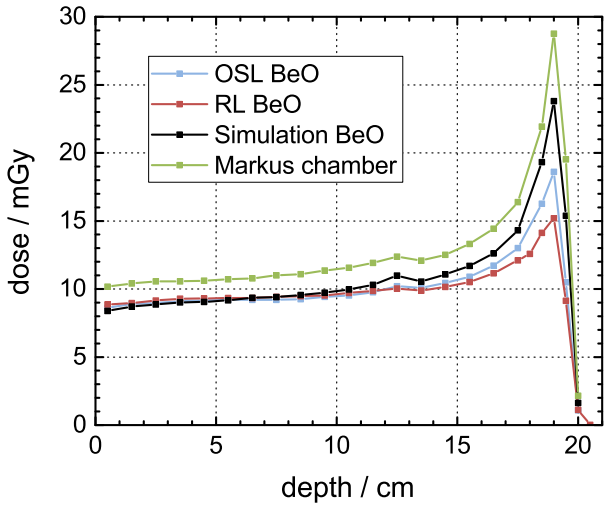

Figure 6. Dose depth curve comparison: OSL and RL measurement and simulation of the dose in BeO. Markus chamber as reference.

3.3 Quenching

To quantify the effect of quenching in BeO, the measured dose values (OSL and RL) are divided by the simulated values. The results are displayed in figure 7. In general, the curves for OSL and RL show the same behaviour. Both ratios start slightly above one and decrease with increasing depth, i.e. with increasing LET. The deviation from the strictly monotonous character at 12.5 cm depth can be explained by the presence of the second lower energy component in the proton spectrum.

Since both curves show a different slope, the quenching of the OSL signal differs from the quenching of the RL measurement. This feature can be exploited to correct for the quenching effect, without knowing the LET. The ratio of the OSL to the RL value shows a direct correlation to the amount of quenching, as displayed in figure 8 vs. the ratio of the reference dose (measured with the ionization chamber) per measured OSL dose. The data has been approximated by a second-order polynomial. The deviation in the lower left of the graph is caused by the lower energy component.

Using the correlation displayed in figure 8 a quenching correction of any measurement can be applied by the following steps. First perform the OSL and RL measurement at a certain depth and determine the ratio of the dose obtained by OSL D_{OSL} to the dose from the RL measurement D_{RL}. This ratio is a monotonous function f of $D_{\mathrm{PMMA}}/D_{\mathrm{OSL}}$

$$\frac{D_{\mathrm{OSL}}}{D_{\mathrm{RL}}} = f\left(\frac{D_{\mathrm{PMMA}}}{D_{\mathrm{OSL}}}\right)$$

as displayed in figure 8. The reference dose D_{PMMA} can then be calculated using the inverse function f^{-1} by

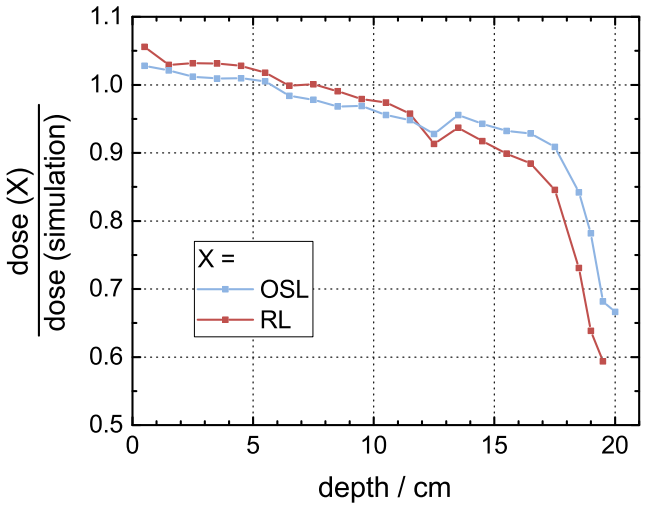

Figure 7. Quenching in dose measurements using the OSL and RL of BeO. Measured dose values obtained by OSL and RL divided by simulated dose in BeO vs. depth in the phantom.

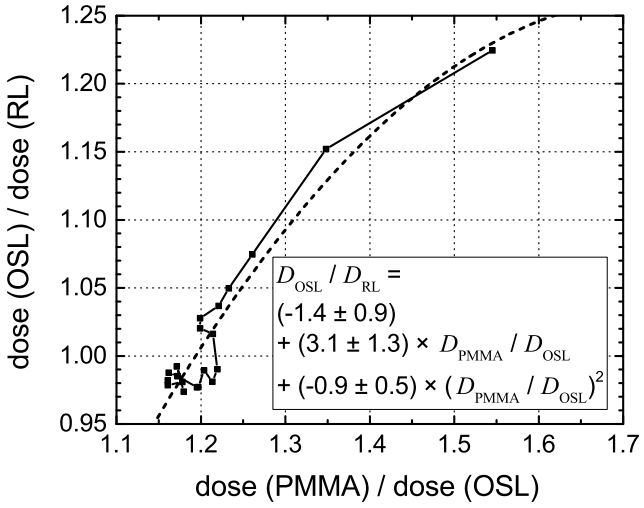

Figure 8. Ratio between the OSL and RL dose vs. the ratio of the reference dose and the OSL dose.

$$D_{\mathrm{PMMA}} = f^{-1}\left(\frac{D_{\mathrm{OSL}}}{D_{\mathrm{RL}}}\right) \cdot D_{\mathrm{OSL}}.$$

It represents the dose in PMMA without any quenching effect. The result of the procedure is plotted in figure 9. In this example the OSL data which is corrected is the very same which is used to obtain the correlation curve in figure 8. Therefore the result is obvious and the figure only serves demonstrative purposes. However the method can be applied universally to any set of OSL/RL data.

According to the Birks' model, the quenching has its cause in the increase in LET. This is the

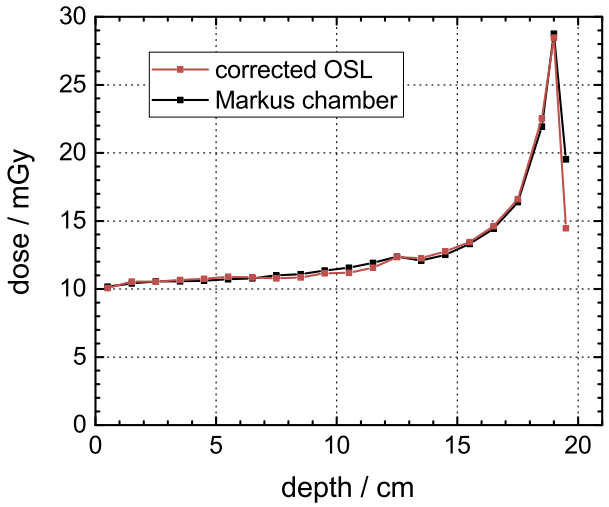

Figure 9. Result of the quenching correction (exemplary): corrected OSL vs. Markus chamber measurement.

motivation to investigate the OSL and RL signal ratio in dependence of the stopping power, which is accessible via simulation only. Under Bragg-Gray conditions, the dose due to primary protons is proportional to the stopping power. The major difference between the proton dose and the total dose is in the entrance path (cf figure 4). Figure 10 displays the measured OSL/RL ratio vs. the simulated dose generated by protons. There is a strong linear correlation and the second order deviation from a linear function has been straightened out. The deviations at 11 mGy might be caused by the fact that this approach neglects that even the neutron dose is caused by recoil protons of a broad energy spectrum. The OSL/RL ratio appears under these conditions as a good measure for the proton stopping power which can be transferred to residual range in a monoenergetic field.

4 Conclusion

Both the OSL and RL of BeO show a dependency on the dose delivered by an MeV proton beam. In the low LET range of the entrance path up to 10 cm depth the two methods deliver the correct absorbed dose. With increasing LET quenching effects cause an underestimation of the dose compared to an ionization chamber reference. The combined use of OSL and RL with different quenching characteristics makes it possible to correct dose readings to an unquenched signal in a given radiation field and thereby also accounting for a transition to dose in another material, e.g. from BeO to PMMA in this case. The investigation of the OSL to RL ratio in dependence of the (simulated) proton only dose suggests, that the ratio might be a useful measure to accurately determine the residual proton range in monoenergetic proton fields.

Further investigations in a clean and monoenergetic radiation field will allow to study the feasibility of combined OSL and RL measurements to determine the range and dose. If it can be shown that this is possible within clinically required limits, this technique can improve the quality assurance especially in scanned proton fields, where individual pencil beam spots can be verified

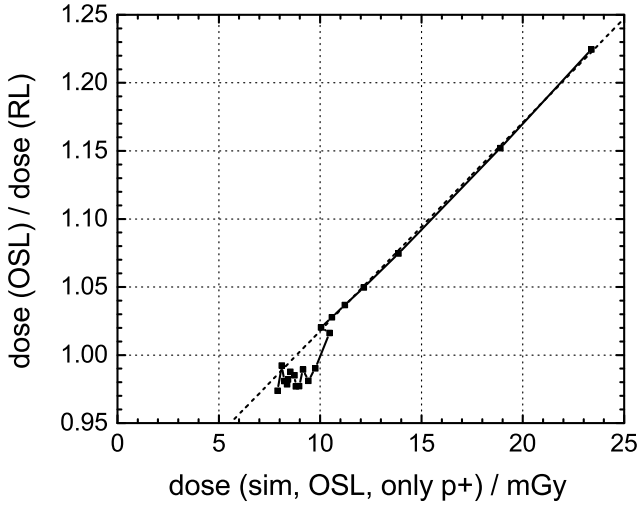

Figure 10. Dose measured by OSL per dose measured using the RL of BeO vs. simulated proton dose in BeO.

not only in terms of absolute dose but also in residual range from a dosimeter placed in the entrance path.

An important practical goal for the applicability is the integration of the two measurement approaches into one combined OSL/RL system.

A Appendix

The following table lists all dose measurements with the OSL chips. The uncertainty (2σ) given for the OSL readings are calculated based on the statistical character of the measurement and the corresponding calibration.

Acknowledgments

This project has received funding from the European Union's Horizon 2020 research and innovation programme under grand agreement No. 654002.

M.J. Gonzalez Torres received support from the DAAD-CONACYT programme under grant No. 50017046.

Table 1. OSL data.

Position / cm	OSL dose / mGy	Position / cm	OSL dose / mGy	Position / cm	OSL dose / mGy
0.575	8.79 ± 0.16	1.575	8.87 ± 0.16	2.575	8.95 ± 0.16
	8.70 ± 0.16		8.81 ± 0.16		8.92 ± 0.16
	8.57 ± 0.15		8.94 ± 0.16		8.99 ± 0.16
	8.68 ± 0.15		8.86 ± 0.16		8.91 ± 0.16
	8.60 ± 0.15		8.77 ± 0.16		8.87 ± 0.16
	8.59 ± 0.15		8.93 ± 0.16		9.00 ± 0.16
	8.58 ± 0.15		8.97 ± 0.16		8.98 ± 0.16
	8.57 ± 0.15		8.90 ± 0.16		8.98 ± 0.16
	8.59 ± 0.15		8.97 ± 0.16		9.15 ± 0.16
3.575	9.09 ± 0.16	4.575	9.18 ± 0.16	5.575	9.17 ± 0.16
	9.00 ± 0.16		9.09 ± 0.16		9.13 ± 0.16
	9.07 ± 0.16		9.13 ± 0.16		9.24 ± 0.17
	9.05 ± 0.16		9.12 ± 0.16		9.14 ± 0.16
	8.98 ± 0.16		9.09 ± 0.16		9.17 ± 0.16
	9.14 ± 0.16		9.12 ± 0.16		9.32 ± 0.17
	9.14 ± 0.16		9.18 ± 0.16		9.28 ± 0.17
	9.10 ± 0.16		9.15 ± 0.16		9.28 ± 0.16
	9.26 ± 0.16		9.24 ± 0.16		9.42 ± 0.17
6.575	9.09 ± 0.16	7.575	9.16 ± 0.16	8.575	9.26 ± 0.16
	9.11 ± 0.16		9.11 ± 0.16		9.19 ± 0.16
	9.10 ± 0.16		9.22 ± 0.17		9.21 ± 0.16
	9.11 ± 0.16		9.18 ± 0.16		9.19 ± 0.16
	9.09 ± 0.16		9.16 ± 0.16		9.18 ± 0.16
	9.13 ± 0.16		9.23 ± 0.16		9.29 ± 0.16
	9.33 ± 0.16		9.17 ± 0.16		9.26 ± 0.16
	9.40 ± 0.17		9.30 ± 0.17		9.36 ± 0.16
	9.40 ± 0.17		9.30 ± 0.16		9.40 ± 0.17
9.575	9.39 ± 0.17	10.575	9.49 ± 0.16	11.575	9.92 ± 0.17
	9.57 ± 0.17		9.46 ± 0.16		9.74 ± 0.17
	9.35 ± 0.17		9.50 ± 0.16		9.67 ± 0.17
	9.36 ± 0.16		9.43 ± 0.16		9.64 ± 0.17
	9.45 ± 0.17		9.48 ± 0.17		9.75 ± 0.17
	9.44 ± 0.17		9.53 ± 0.17		9.81 ± 0.17
	9.44 ± 0.17		9.59 ± 0.17		9.72 ± 0.17
	9.59 ± 0.17		9.60 ± 0.17		9.87 ± 0.17
	9.46 ± 0.16		9.69 ± 0.17		9.84 ± 0.17
12.575	10.17 ± 0.18	13.575	10.09 ± 0.18	14.575	10.33 ± 0.18
	10.12 ± 0.18		10.17 ± 0.18		10.38 ± 0.18
	10.17 ± 0.18		10.23 ± 0.18		10.37 ± 0.18
	10.14 ± 0.18		10.00 ± 0.18		10.36 ± 0.18
	10.10 ± 0.18		10.04 ± 0.18		10.45 ± 0.18
	10.21 ± 0.18		10.12 ± 0.18		10.57 ± 0.18
	10.21 ± 0.18		10.04 ± 0.18		10.46 ± 0.18
	10.30 ± 0.18		10.03 ± 0.18		10.56 ± 0.18
	10.38 ± 0.18		10.05 ± 0.18		10.51 ± 0.18
15.575	10.79 ± 0.19	16.575	11.56 ± 0.21	17.575	12.9 ± 0.2
	10.80 ± 0.19		11.68 ± 0.21		13.0 ± 0.2
	10.87 ± 0.19		11.57 ± 0.21		12.8 ± 0.2
	10.82 ± 0.20		11.53 ± 0.21		12.9 ± 0.2
	10.91 ± 0.19		11.65 ± 0.21		13.0 ± 0.2
	10.98 ± 0.20		11.86 ± 0.21		13.1 ± 0.2
	10.88 ± 0.19		11.83 ± 0.21		13.0 ± 0.2
	10.96 ± 0.19		11.85 ± 0.21		13.0 ± 0.2
	11.07 ± 0.20		11.87 ± 0.21		13.1 ± 0.2
18.575	16.4 ± 0.2	19.075	18.4 ± 0.3	19.575	10.56 ± 0.19
	16.1 ± 0.2		18.6 ± 0.3		10.24 ± 0.19
	16.1 ± 0.2		18.6 ± 0.3		10.50 ± 0.18
	16.2 ± 0.2		18.5 ± 0.3		10.46 ± 0.18
	16.2 ± 0.2		18.8 ± 0.3		10.24 ± 0.18
	16.2 ± 0.2		18.7 ± 0.3		10.58 ± 0.18
	16.3 ± 0.2		18.6 ± 0.3		10.69 ± 0.19
	16.5 ± 0.2		18.6 ± 0.3		10.49 ± 0.19
	16.5 ± 0.2		18.7 ± 0.3		10.65 ± 0.19
20.075	1.12 ± 0.02				
	1.01 ± 0.02				
	1.10 ± 0.02				
	1.07 ± 0.02				
	0.97 ± 0.02				
	1.09 ± 0.02				
	1.19 ± 0.02				
	1.06 ± 0.02				
	1.17 ± 0.02				

References

[1] IAEA, *Absorbed dose determination in external beam radiotherapy: An international code of practice for dosimetry based on standards of absorbed dose to water*. Technical Report Series No. 398, 2000.

[2] L. A. Perles, D. Mirkovic, A. Anand, U. Titt and R. Mohan, *LET dependence of the response of EBT2 films in proton dosimetry modeled as a bimolecular chemical reaction*, *Phys. Med. Biol.* **58** (2013) 8477.

[3] H. Palmans, *Effect of alanine energy response and phantom material on depth dose measurements in ocular proton beams*, *Technol. Cancer Res. Treat.* **2** (2003) 579–586.

[4] H. Gustavsson, S. r. J. Bäck, J. Medin, E. Grusell and L. E. Olsson, *Linear energy transfer dependence of a normoxic polymer gel dosimeter investigated using proton beam absorbed dose measurements*, *Phys. Med. Biol.* **49** (2004) 3847.

[5] L. Raffaele, *Advances in hadrontherapy dosimetry*, *Phys. Med.* **32** (2016) 187.

[6] F. Marsolat, L. D. Marzi, A. Patriarca, C. Nauraye, C. Moignier, M. Pomorski et al., *Dosimetric characteristics of four PTW microDiamond detectors in high-energy proton beams*, *Phys. Med. Biol.* **61** (2016) 6413.

[7] G. Scarpa, *The dosimetric use of beryllium oxide as a thermoluminescent material: A preliminary study*, *Phys. Med. Biol.* **15** (1970) 667.

[8] E. Bulur and H. Y. Göksu, *OSL from BeO ceramics: new observations from an old material*, *Radiat. Meas.* **29** (1998) 639–650.

[9] E. G. Yukihara, *Luminescence properties of BeO optically stimulated luminescence (OSL) detectors*, *Radiat. Meas.* **46** (2011) 580–587.

[10] A. Jahn, M. Sommer and J. Henniger, *OSL efficiency for BeO OSL dosimeters*, *Radiat. Meas.* **71** (2014) 104–107.

[11] M. Sommer and J. Henniger, *Investigation of a BeO-based optically stimulated luminescence dosemeter*, *Radiat. Prot. Dosim.* **119** (2006) 394–397.

[12] M. Sommer, R. Freudenberg and J. Henniger, *New aspects of a BeO-based optically stimulated luminescence dosimeter*, *Radiat. Meas.* **42** (2007) 617–620.

[13] M. Sommer, A. Jahn and J. Henniger, *Beryllium oxide as optically stimulated luminescence dosimeter*, *Radiat. Meas.* **43** (2008) 353–356.

[14] A. Jahn, M. Sommer and J. Henniger, *2d-OSL-dosimetry with beryllium oxide*, *Radiat. Meas.* **45** (2010) 674–676.

[15] A. Jahn, M. Sommer, M. Liebmann and J. Henniger, *Progress in 2d-OSL-dosimetry with beryllium oxide*, *Radiat. Meas.* **46** (2011) 1908–1911.

[16] M. Sommer, A. Jahn and J. Henniger, *A new personal dosimetry system for $h_P(10)$ and $h_P(0.07)$ photon dose based on OSL-dosimetry of beryllium oxide*, *Radiat. Meas.* **46** (2011) 1818–1821.

[17] A. Jahn, M. Sommer, W. Ullrich, M. Wickert and J. Henniger, *The BeOmax system – dosimetry using OSL of BeO for several applications*, *Radiat. Meas.* **56** (2013) 324–327.

[18] A. Jahn, M. Sommer and J. Henniger, *Environmental dosimetry with the BeOSL personal dosimeter – state of the art*, *Radiat. Meas.* **71** (2014) 438–441.

[19] A. M. C. Santos, M. Mohammadi, J. Asp, T. M. Monro and S. Afshar V., *Characterisation of a real-time fibre-coupled beryllium oxide (BeO) luminescence dosimeter in x-ray beams*, *Radiat. Meas.* **53-54** (2013) 1–7.

[20] A. M. C. Santos, M. Mohammadi and S. Afshar V., *Investigation of a fibre-coupled beryllium oxide (BeO) ceramic luminescence dosimetry system*, *Radiat. Meas.* **70** (2014) 52–58.

[21] T. Teichmann, J. Sponner, C. Jakobi and J. Henniger, *Real time dose rate measurements with fiber optic probes based on the RL and OSL of beryllium oxide*, *Radiat. Meas.* **90** (2016) 201–204.

[22] J. B. Birks, *Scintillations from organic crystals: Specific fluorescence and relative response to different radiations*, *Proc. Phys. Soc. A* **64** (1951) 874.

[23] J. B. Birks, *The theory and practice of scintillation counting*, vol. 27 of *International series of monographs on electronics and instrumentation*. Pergamon Press, London U.K., 1964.

[24] V. I. Tretyak, *Semi-empirical calculation of quenching factors for ions in scintillators*, *Astropart. Phys.* **33** (2010) 40–53.

[25] S. Brandenburg, *The superconducting cyclotron AGOR: Accelerator for light and heavy ions*, *Proceedings of the 1987 IEEE particle accelerator conference: Accelerator engineering and technology* (1987) .

[26] S. Brandenburg, R. Ostendorf, M. Hofstee, H. Kiewiet and H. Beijers, *The irradiation facility at the AGOR cyclotron*, *Nucl. Instrum. Methods Phys. Res. B* **261** (2007) 82–85.

[27] J. Radtke, J. Sponner, C. Jakobi, J. Schneider, M. Sommer, T. Teichmann et al., *Single photon detection and signal analysis for high sensitivity dosimetry based on optically stimulated luminescence with beryllium oxide*, *EPJ Web Conf.* **170** (2018) 09009.

[28] T. T. Böhlen, F. Cerutti, M. P. W. Chin, A. Fassò, A. Ferrari, P. G. Ortega et al., *The FLUKA code: Developments and challenges for high energy and medical applications*, *Nucl. Data Sheets* **120** (2014) 211–214.

[29] A. Ferrari, P. R. Sala, A. Fassò and J. Ranft, *FLUKA: A multi-particle transport code*. CERN Yellow Reports CERN 2005-10, INFN/TC_05/11, SLAC-R-773, 2005.

[30] M. Berger, J. Coursey, M. Zucker and J. Chang, "Stopping-power & range tables for electrons, protons, and helium ions - NIST standard reference database 124." `https://www.nist.gov/pml/stopping-power-range-tables-electrons-protons-and-helium-ions` [Accessed: 2018-07], 2009.

[31] SR-NIEL, "Protons & ions nuclear stopping power calculator." `http://www.sr-niel.org/index.php/protons-ions-nuclear-stopping-power-calculator` [Accessed: 2018-07], 2017.